Asymmetric domain wall propagation caused by interfacial Dzyaloshinskii-Moriya interaction in exchange biased Au/Co/NiO layered system

P. Kuświk,[1,*] M. Matczak,[1] M. Kowacz,[2] K. Szuba-Jabłoński,[3] N. Michalak,[1] B. Szymański,[1] A. Ehresmann,[4] and F. Stobiecki[1]

[1]*Institute of Molecular Physics, Polish Academy of Sciences, Smoluchowskiego 17, 60-179 Poznań, Poland*

[2]*Faculty of Technical Physics, Poznań University of Technology, Piotrowo 3, 60-965 Poznań, Poland*

[3]*Department of Physics, College of Science, Swansea University, Singleton Park, Swansea SA2 8PP, United Kingdom*

[4]*Institute of Physics and Center for Interdisciplinary Nanostructure Science and Technology (CINSaT), University of Kassel, Heinrich-Plett-Str. 40, D-34132 Kassel, Germany*

(Received 23 March 2017; published 3 January 2018)

Dzyaloshinskii-Moriya interaction (DMI) is a well-known phenomenon in ferromagnetic/heavy metal or ferromagnetic/nonmagnetic oxide thin layered films. Here, we show that DMI is also found in exchange biased ferromagnetic/antiferromagnetic oxide layer systems and that it is independent of the macroscopic direction of the interlayer exchange bias coupling. Using the relation between thickness of the ferromagnetic layer and asymmetric domain wall propagation at external magnetic fields applied in plane and perpendicular to a sample plane of a Au/Co/NiO layered system, the strength of interfacial Dzyaloshinskii-Moriya interaction was determined. Based on this relation, we found that observed clockwise chirality is related to strong negative Dzyaloshinskii-Moriya interaction, which is independent of the direction of the interlayer exchange bias coupling. We also demonstrate that in the Au/Co/NiO system, domain motion can be controlled precisely by alternating magnetic fields. This concept can be attractive for many applications based on field-induced domain and domain wall motion, particularly in systems where exchange bias is required.

DOI: 10.1103/PhysRevB.97.024404

I. INTRODUCTION

The asymmetric exchange interaction, known as Dzyaloshinskii-Moriya interaction (DMI) [1,2], was examined to explain chiral spin configurations [3,4]. It is widely investigated in thin layered systems with perpendicular magnetic anisotropy (PMA) because it allows to fabricate magnetic recording media with extremely high data storage densities and offers concepts of an information technology based on skyrmion or current-induced domain or domain wall (DW) motion [5,6]. The DMI in layered systems is induced by the inversion symmetry breaking at interfaces causing noncollinear spin configuration mediated by atoms with a large spin-orbit coupling (SOC) [7]. The energy term associated with DMI can be expressed as $E_{\mathrm{DM}} = \vec{D} \cdot (\vec{S}_1 \times \vec{S}_2)$, where $\vec{S}_1$ and $\vec{S}_2$ denote the atomic spins and $\vec{D}$ is the Dzyaloshinskii-Moriya vector, which is proportional to the SOC constant and correlates the positions of two magnetic transition-metal atoms and a mediating atom [7,8]. In films with PMA, the DMI may stabilize Néel-type domain walls (N-DWs) because the resulting vector of $(\vec{S}_1 \times \vec{S}_2)$ is parallel to $\vec{D}$. In Bloch-type DWs and N-DWs in thin films with in-plane anisotropy, this cross-product is perpendicular to $\vec{D}$ and, as a consequence, E_{DM} is zero (Fig. 2 in [9]). Note that in thin ferromagnetic films, other interactions can force different domain wall types even when DMI is present [10].

The chirality of the spin configuration in skyrmions or skyrmion bubbles (cylindrical domains with uniform magnetization arrangements in their centers and spin chiralities characterized by winding numbers $W = |1|$) is determined by $\vec{D}$. Therefore, research is focused on the strength and the sign of the Dzyaloshinskii-Moriya constant (D), which is crucial to control current- or field-driven DW propagation in multilayers (MLs) characterized by PMA and DMI. Here, negative D describes clockwise chirality. Very recently, it was shown that using alternating homogeneous external magnetic fields, the remote control of skyrmionlike domain propagation is possible in films characterized by both PMA and DMI due to the presence of N-DWs [11,12]. This approach opens a new way to build magnetic memories based on the racetrack memory principle, where domain positions can be controlled by alternating magnetic fields [11].

Currently, the most studies are carried out for thin layered films with two or more interfaces between heavy metals (HM) and transition-metal ferromagnets (FM) (Table I in Ref. [13]) because the interlayer exchange coupling in metallic ML stacks can stabilize skyrmion-type domains at room temperature without external magnetic field [14]. Particular attention has been paid to asymmetric interfaces (e.g., Pt/Co/Ir), where the DMI is strongly enhanced [15], if the FM layer is sandwiched between two different HM layers providing additive chiral interactions, enhancing the effective DMI ($\vec{D}_{\mathrm{eff}}$) [16]. It is also known that using oxides (e.g., MgO) replacing one of the HM layers increases absolute magnitude of the DMI constant about 1.6 times [15] and enables a DMI strength control by oxide coverage [9]. The interest in layered film system capped by an insulator (e.g., MgO, Al_2O_3) is motivated by possible future applications (e.g., magnetic tunnel junctions), where DMI may play an essential role in the magnetization reversal process [17]. Additionally, the insulator capping layer may be used to tune magnetization switching by an electric field [18], which

*kuswik@ifmpan.poznan.pl

reduces power consumption in future devices. Therefore, we have investigated the DMI in a HM/FM/antiferromagnetic insulator (NiO) layer system, possessing an additional degree of freedom for magnetic property tuning, namely, the perpendicular exchange bias in the present case. This may be particularly important for future racetrack memories based on magnetic domain wall motion [19], where the antiferromagnetic (AFM) layer is coupled with the FM layer through an interlayer exchange bias coupling (IEBC), which can be used as pinning sites [20] for stabilization and optimization of the DW movement [19,21].

We show that in an Au/Co/NiO exchange biased layer system, Néel domain walls are stabilized by DMI. The chirality and strength of the DMI was determined from polar magneto-optical Kerr effect (PMOKE) measurements, where out-of-plane and in-plane magnetic fields (H_z and H_x, respectively) were applied.

Based on these results and experiments described by Moon *et al.* [11], a magnetic field sequence (combination of H_z and H_x fields) has been established to move a skyrmionic bubble domain along the x direction over a distance of tens of microns, indicating a controllable domain motion. Possible applications of this effect include the transport of properly functionalized magnetic beads, trapped by the magnetostatic field over the DWs or domains (in the case where the domain is small in comparison to the size of the beads), in lab-on-a-chip devices [22–25]. This phenomenon can be applied to fluid mixing by moving particles [26] or in data storage based on shift registers [27].

II. EXPERIMENTAL DETAILS

Uniform buffer/Au/Co-t_{Co}/NiO/Au layer systems were prepared in a multichamber system with base pressure below 2×10^{-8} mbar. Various Ti/Au buffers on naturally oxidized Si substrates ensured perpendicular anisotropy of the Co layer [28]. The Ti, Au, and Co layers were deposited by magnetron sputtering in Ar atmosphere at $p_{Ar} = 1.4 \times 10^{-3}$ mbar and the NiO layer was deposited using pulsed laser deposition in an oxygen atmosphere at $p_O = 1.5 \times 10^{-5}$ mbar for correct stoichiometry [29]. All layers were deposited at room temperature. The deposition processes were realized in separate vacuum chambers and samples were transferred between them without breaking vacuum conditions. The samples were deposited in an external magnetic field of $H_{dep} = 1.1$ kOe, oriented perpendicularly to the sample plane, to initialize the perpendicular IEBC between the Co and the NiO layers [30]. The role of the direction of IEBC on the spin chirality at the interfaces of the system has been investigated for two different field-cooling (FC) processes performed in N_2 atmosphere from 373 K down to room temperature (RT) in $H_{FC^+} = +5$ kOe and $H_{FC^-} = -5$ kOe, applied perpendicularly to the sample plane. Local hysteresis loops were measured using a PMOKE magnetometer with a laser spot diameter of ~0.3 mm. Images of the magnetic domains were recorded using a PMOKE wide microscope. Note that for hysteresis loop measurements the magnetic field was swept and for the domain observations it was applied in pulses causing small differences between switching fields determined by both methods. X-ray photoelectron spectroscopy (XPS) measurements were carried out in a separate UHV chamber using a nonmonochromatic Al K_α (1.486 eV) x-ray radiation source and a hemispherical electron energy analyzer. Pass energies of 50 (survey spectra) and 20 (regions) eV were applied. The exact binding energies were determined by shifting the spectra with respect to the C 1s peak at 284.8 eV [31], which is related to ambient exposure contamination. The spectra were fitted using the CasaXPS software (Casa

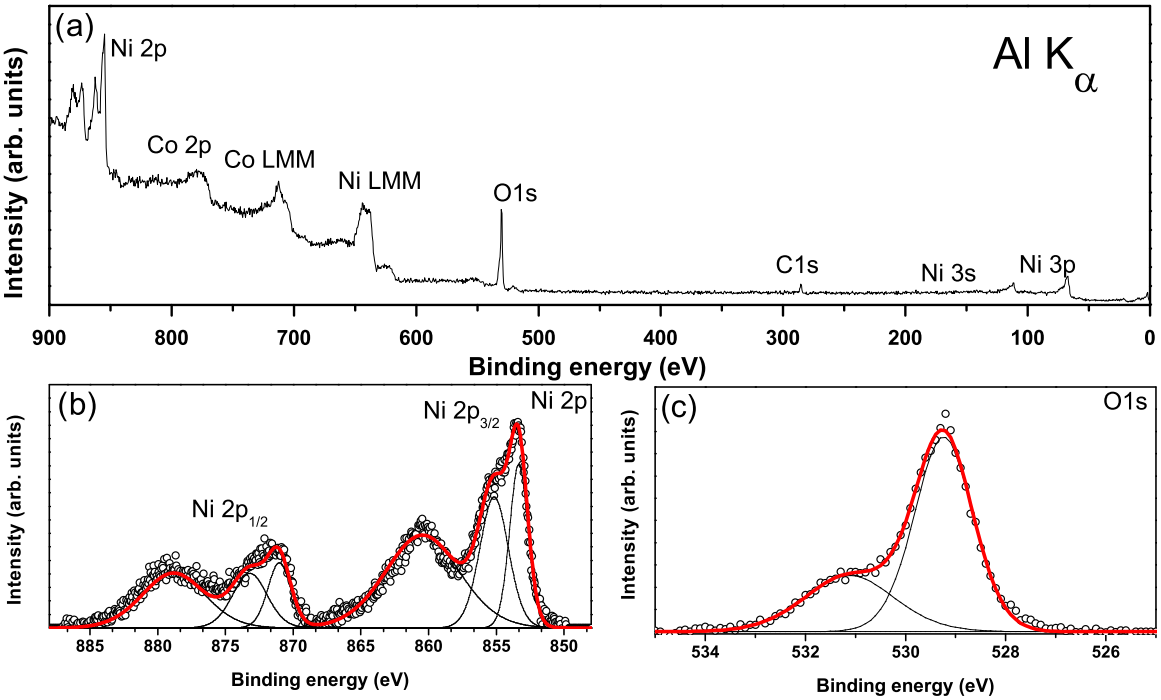

FIG. 1. (a) X-ray photoelectron survey spectrum of the Ti-4 nm/Au-60 nm/Co-2 nm/NiO-10 nm sample recorded using Al K_α x-ray radiation. Region x-ray photoelectron spectra for (b) Ni 2p and (c) O 1s.

Software Ltd) using Voigt functions and Shirley background subtraction. Quantitative analysis was performed by taking the photoionization cross-section parameters of the respective elements into account [32]. All measurements were performed at RT.

III. RESULTS AND DISSCUSION

The XPS survey scan of the Ti-4 nm/Au-60 nm/Co-2 nm/NiO-10 nm sample is shown in Fig. 1(a). The spectrum revealed the presence of cobalt, nickel, and oxygen in the sample, as well as carbon related to ambient contamination. Due to the limited probing depth of XPS, which is on the order of a few nanometers, signals originating from Au, Ti, and Si could not be detected. The quantitative analysis revealed a Ni(35%)/O(45%)/Co(11%)/C(9%) composition (concentration given in at. %) of the studied sample.

In order to determine the chemical state of the main elements, we fitted the Ni $2p$ and O $1s$ regions [shown in Figs. 1(b) and 1(c), respectively] and analyzed the binding energy shifts of the fitted components. The Ni $2p$ region was fitted with six components. Two main peaks, centered at 853.4 and 871.1 eV [33], indicated the presence of nickel in the Ni^{2+} oxidation state. This was further confirmed by the presence of two characteristic satellite peaks centered at 860.5 and 879.0 eV [34]. Following the approach of Grosvenor *et al.* [35], we also added two additional components in order to level the valleys between the main peaks and the satellites. According to Hagelin-Weaver *et al.*, these additional peaks can be attributed to the interband losses [36,37].

The O $1s$ region was best-fitted with two components: The high-intensity peak (approximately 70% of the total oxygen content) was centered at around 529.3 eV and assigned to originate from NiO [33]. The low intensity component, centered at 531.1 eV, was assigned to originate from surface adsorbates (e.g., CO on NiO [38]). Taking into account the amount of oxygen originating from NiO, the total amount of nickel in the sample, and the fact that all the nickel was in the Ni^{2+} oxidation state, the results proved that our pulsed laser deposition procedure ensures stoichiometry [29] and therefore the antiferromagnetic phase of the NiO layer at RT.

Figure 2 shows the PMOKE hysteresis loops for the as-deposited (Ti-4 nm/Au-4 nm)$_5$/Co-0.54 nm/NiO-10 nm/Au-2 nm ML and after the FC processes. In all cases, a rectangular hysteresis loop proves PMA and that magnetization reversal takes place by domain nucleation followed by DW propagation, which will be discussed in detail below. The shift of the hysteresis loop center from zero field reveals the presence of IEBC between the Co and NiO layers. In our case, this shift is opposite to the direction of the magnetic field applied during the deposition or the FC process (Fig. 2). The possibility to investigate samples with a different direction of IEBC [positive or negative exchange bias (H_{EB})] opens a way to investigate a possible correlation between DMI and IEBC.

For the current thin film, the DW propagation caused by pulses of H_z applied simultaneously with a constant H_x field was systematically investigated for different signs of H_{EB}. The field-induced DW displacements were recorded using PMOKE microscopy and the results for an as-deposited sample are shown in Fig. 3. For nucleation of an initial bubble domain,

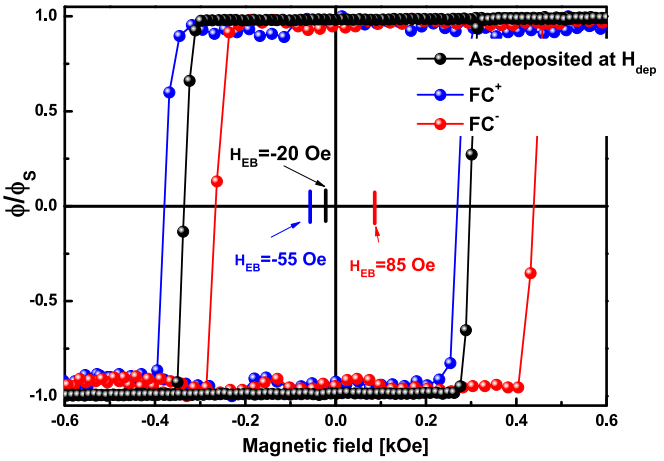

FIG. 2. PMOKE hysteresis loops measured for (Ti-4 nm/Au-4 nm)$_5$/Co-0.54 nm/NiO-10 nm/Au-2 nm ML in the as-deposited state deposited in an external magnetic field of $H_{dep} = 1.1$ kOe (black) and after FC in $H_{FC^+} = 5$ kOe and $H_{FC^-} = -5$ kOe (blue and red, respectively). For each loop, H_{EB} is marked.

the sample has been magnetically saturated by a field pulse of $H_z = -2000$ Oe (2000 Oe) for 1 s followed by a field pulse of $H_z = +275$ Oe (-330 Oe) for 1 s. The corresponding PMOKE microscope images in remanence have been taken as reference images and are not shown in Fig. 3, but the originally nucleated domains are marked by a pink arrow in the difference images. The reference image showed only one nucleated domain, but as can be seen in the difference images of Fig. 3, more domains are nucleated in the course of the experiments. We will now focus on the evolution of the originally nucleated domain when a static in-plane magnetic field of $H_x = 900$ Oe (-900 Oe) is applied together with a sequence of perpendicular to plane magnetic field pulses H_z of $+275$ Oe [Figs. 3(a) and 3(b)] and of -330 Oe [Figs. 3(c) and 3(d)] for 1 s each. After each pulse, a PMOKE microscope image has been taken in remanence and the differences to the respective reference images after the first four pulses of H_z are displayed in Fig. 3. Note that using the same H_z field pulses as for the initial nucleation, the domain slightly expanded, enabling to observe the domain evolution. For a domain nucleated by the field pulse in $+z$ direction, a static applied magnetic field in $+/-$ x direction results in an anisotropic expansion of the domain with preference for the $+/-$ x directions, respectively, or in other words results in a shift of the domain's center in $+/-$ x direction, respectively. However, that was only observed when the magnetization inside the domain was oriented up (positive H_z field pulses) [Figs. 3(a) and 3(b)]. For a reversed orientation of magnetization in the center of the domain (negative H_z field pulse), the domain expands in the opposite direction [Figs. 3(c) and 3(d)]. The asymmetric expansion of the domain in $+/-$ x direction is caused by the additional Zeeman energy induced by the applied constant in-plane field H_x. The N-DW energy is lower for a magnetic field parallel to the resultant magnetization inside the DW (DW1) and higher for antiparallel alignment (DW2). Because the DW speed depends on the DW energy [39,40], a skyrmionlike domain expands anisotropically in the presence of a combination of H_z and H_x magnetic fields (Fig. 3).

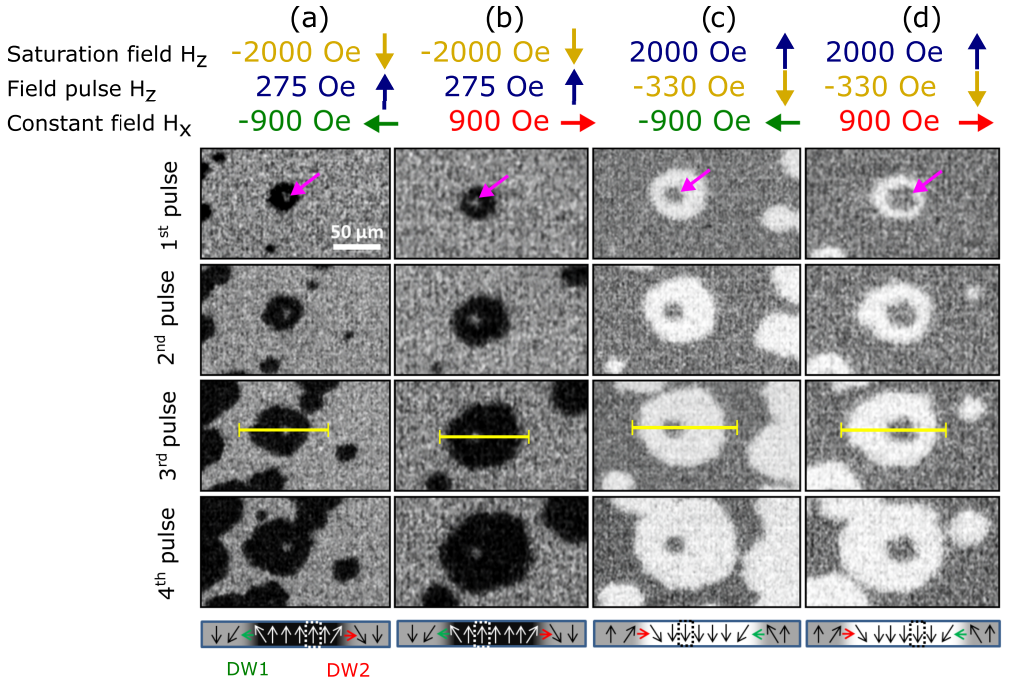

FIG. 3. PMOKE difference images of the domain evolution for the (Ti-4 nm/Au-4 nm)$_5$/Co-0.54 nm/NiO-10 nm/Au-2 nm ML in combined constant in-plane field [(a), (c) $H_x = -900$ Oe and (b), (d) $H_x = 900$ Oe] and perpendicular to plane field pulses ($\Delta\ t = 1$ s) [(a),(b) $H_z = +275$ Oe and (c), (d) $H_z = -330$ Oe] after saturation in (a), (b) $H_z = -2000$ Oe and (c), (d) $H_z = +2000$ Oe. Pink arrows mark the initial position of the nucleated domain. In the lowermost panels, the spin configurations along the yellow lines are schematically drawn. DW1 and DW2 indicate the N-DW with clockwise chirality, in which the resultant magnetization inside the DW is parallel and antiparallel to the direction of H_x, respectively.

Our results show that in the Au/Co/NiO system, the spin configuration in the DW has clockwise chirality (Fig. 3), which is related to a negative effective DMI constant (D_{eff}) [8]. Note that in all investigated cases, the DW1 moves approximately 1.7 times faster than DW2, irrespective whether as-deposited samples have been used or the samples have been field cooled. The propagation asymmetry of the domain walls along the x coordinate in the regime of creep domain wall motion was used to determine the strength of the interfacial DMI for different Co layer thicknesses [Fig. 4(a)]. We found that the DW has clockwise chirality for all Co layer thicknesses [confirmed also by the monotonic dependence shown in Fig. 4(a)]. For large t_{Co} (e.g., $t_{\text{Co}} = 1.1$ nm), i.e., in the vicinity of the spin-reorientation transition from out of plane to in plane, the DW2 moves only slightly as compared with DW1. To analyze this behavior, we determined the asymmetry of the domains expansion by averaging the relative DW displacements x_1 and x_2 [see Fig. 4(a)] over a few domains. Because both domain walls DW1 and DW2 move under the same set of magnetic field pulses for a defined time (τ), the ratio $\frac{x_1}{x_2}$ describes the asymmetry of the DWs velocities by $a = \frac{v_1}{v_2} \equiv \frac{x_1}{x_2}$, where $v_1 = \frac{x_1}{\tau}$ and $v_2 = \frac{x_2}{\tau}$ are the velocities of DW1 and DW2, respectively [Fig. 4(b), black symbols]. The parameter a is the ratio of a creep velocities, which can be described by $v = v_0 \exp[-\kappa(\mu_0 H_z)^{(-1/4)}]$ (v_0 is the characteristic speed and κ is a scaling coefficient) [40]. In using the parameter a to describe the DW velocity asymmetry, v_0 cancels out and therefore the prefactors (correlation length and attempt frequency) responsible for chiral damping [41] are not affecting our analysis. This approach also reduces the number of fitting parameters. The κ can be described [40] as $\kappa = \kappa_0\,[\sigma(H_x)/\sigma_0]^{1/4}$, where κ_0 is a scaling constant and σ is the DW energy density, which is a function of H_x. The $\sigma(H_x)$ can be described as $\sigma(H_x) = \sigma_0 + 2K_D\Delta - \pi\Delta\mu_0 M_S|H_x + H_{\text{DMI}}|$ for N-DW or as $\sigma(H_x) = \sigma_0 - \frac{(\pi\Delta\mu_0 M_S)^2}{8K_D}(H_x + H_{\text{DMI}})^2$ for DW, in which there is no full transformation of the Bloch wall into the N-DW under H_x [39,40]. Here, M_S is the saturation magnetization (for the Co layer we use the bulk value $M_S = 1.4 \times 10^6$ A/m^2 [30]), σ_0 is the Bloch wall energy density, K_D is the DW anisotropy energy density, and Δ is the DW width. Based on the results for a Au/Co/NiO system [42], we expect strong DMI and therefore we used the definition of $\sigma(H_x)$ for an N-DW. In our fitting procedure we used $\Delta = \sqrt{A/K_{\text{eff}}}$, and $\sigma_0 = 2\pi\sqrt{AK_{\text{eff}}}$, where $K_{\text{eff}} = K_V + 2K_S/t_{\text{Co}}$. The volume ($K_V = -1.06$ MJ/m^3) and surface ($K_S = 0.7$ mJ/m^2) components of the effective anisotropy (K_{eff}) were determined in our earlier work [30]. The value of $A = 10$ pJ/m was taken from [16,43]. The magnetostatic shape anisotropy term favoring the Bloch wall is $K_D = N_x\ \mu_0\ M_S^2/2$, where N_x is the demagnetizing coefficient of the DW described by $N_x = t_{\text{Co}}\ln(2)/(\pi\Delta)$ [44]. By using $H_{\text{DMI}} = \frac{D_{\text{eff}}}{\mu_0 M_S \Delta}$, where $D_{\text{eff}} = D_s/t_{\text{Co}}$, we built the relation between a and the thickness of the Co layer, which can be used for fitting our experimental data to obtain the interfacial DMI constant (D_s). Since the increasing thickness of the Co layer influences both the K_{eff} (as a consequence also H_C) and D_{eff}, the measurements of the DW propagation were carried out at different values of H_z and H_x. For different t_{Co} values, H_z and H_x were selected to expand domains of

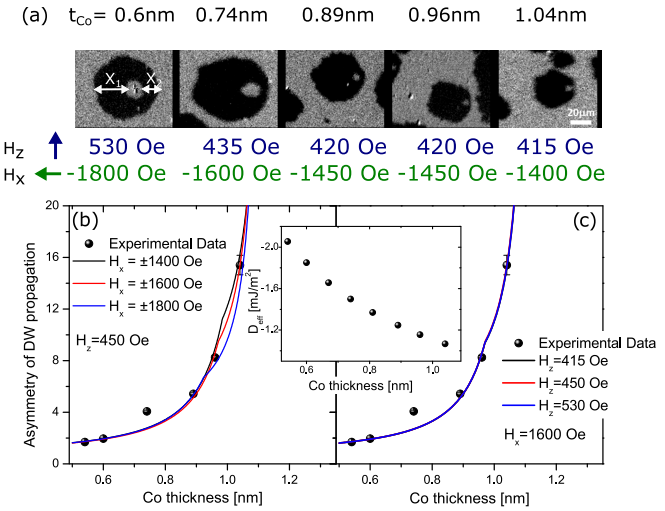

FIG. 4. (a) PMOKE difference images for Ti-4 nm/Au-60 nm/Co-$t_{Co} = 0.6$–1.04 nm/NiO-10 nm/Au-2 nm at in-plane field range $-1400\ \text{Oe} \geqslant H_x \geqslant -1800\ \text{Oe}$ and perpendicular to plane field pulses range $415\ \text{Oe} \leqslant H_z \leqslant 530\ \text{Oe}$ ($\Delta t = 1$ s). (b), (c) Asymmetry parameter a (for definition see text) of domain propagation versus Co thickness obtained from PMOKE images (black symbols). Solid lines represents fitting curve (b) for various H_x and constant H_z and (c) for various H_z and constant H_x. Inset shows the strength of the effective DMI constant as a function of the Co layer thickness assuming that $D_s = -1.11$ pJ/m (see text).

similar sizes [Fig. 4(a)], which allows to determine the a parameter. Subsequently, fits were performed, first keeping the absolute magnitude of pulsed z field and varying H_x [Fig. 4(b)], then keeping the absolute magnitude of the static x field and varying H_z [Fig. 4(c)] fitting are performed. Changes of H_z [Fig. 4(c)] only slightly modify the dependence of $a(t_{Co})$. More pronounced changes of $a(t_{Co})$ are observed with different H_x, particularly in the range of t_{Co} and H_x, for which v_1 is close to zero. In this range, the relationship $a(t_{Co})$ shows a local peculiarity, whose position varies with H_x. For the proposed procedure, only two parameters D_s and κ_0 need to be fitted. The values of these parameters for the five combinations of H_z and H_x are shown in Table I. Particularly important is D_s defining the strength of the interfacial DMI. For a given H_x range, the change of this parameter does not exceed 10% of the average $D_s = -1.11$ pJ/m. Based on this value, the D_{eff} constant can be calculated for each Co thickness (inset in

TABLE I. List of D_s and κ_0 values obtained from fitting for different H_x and H_z magnetic fields.

H_z (Oe)	H_x (Oe)	$\lvert D_s \rvert$ (pJ/m)	κ_0
	1400	1.03 ± 0.05	6.36 ± 0.29
450	1600	1.13 ± 0.05	5.37 ± 0.27
	1800	1.11 ± 0.05	5.11 ± 0.40
415		1.13 ± 0.05	5.26 ± 0.26
450	1600	1.13 ± 0.05	5.37 ± 0.27
530		1.13 ± 0.05	6.60 ± 0.28

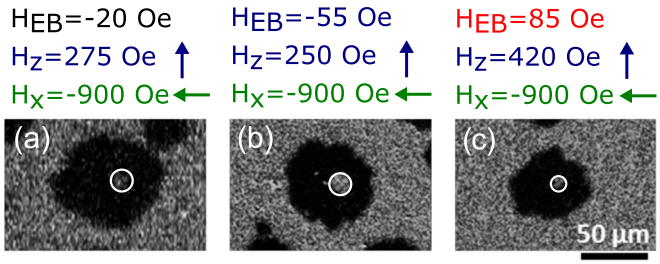

FIG. 5. PMOKE difference images of the domain evolution after three positive magnetic field pulses ($\Delta t = 1$ s) of (a) $H_z = 275$ Oe,(b) $H_z = 250$ Oe,(c) $H_z = 420$ Oe with $H_x = -900$ Oe for (a) as-deposited state (this is the same domain structure as in Fig. 3 after third H_z pulse, (b) FC^+, and (c) FC^- processes. The rings mark the initial position and shape of the domain.

Fig. 4). The obtained values of D_s and therefore D_{eff} are close to that found for asymmetric magnetization reversal studied for triangular microstructures from the same Au/Co/NiO layered system [42].

To investigate the influence of the different IEBC directions on the chirality of the DW, the same PMOKE recording procedure was applied for samples subjected to FC^+ and FC^- processes (Fig. 5). After FC^+ and FC^- the asymmetric domain evolution along the x direction appears in the same way as for the as-deposited sample (Fig. 5). This indicates that the FC process does not change the chirality of N-DW (the sign of the DMI), although the system exhibits the opposite IEBC direction after FC^+ and FC^-. As the velocity ratio of the DW movement is almost the same for as-deposited and FC samples, we conclude that the DMI is independent of IEBC, which is in good agreement with our previous paper [42]. Note that the nucleation of the reversed domain appears at different values of the negative and positive magnetic field pulse for the as-deposited state and after FC, which is related to the IEBC between the antiferromagnet (NiO) and ferromagnet (Co) films. These experiments prove the coexistence of both the EB effect and the DMI, which previously was only

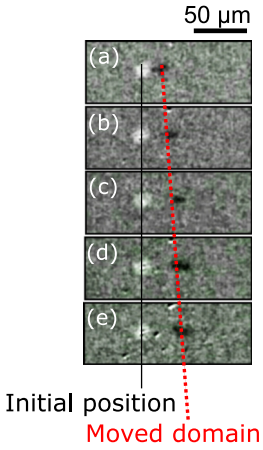

FIG. 6. PMOKE difference images of domain movement after five (a)–(e) cycles of alternating magnetic field ($H_x = +900$ Oe, $H_z = +300$ Oe and $H_x = -900$ Oe, $H_z = -300$ Oe) pulses ($\Delta t = 1$ s) after nucleation of the initial domain with $H_z = +300$ Oe.

theoretically predicted for the IrMn/Co system [45]. Moreover, our experiments indicate that although both IEBC and DMI are interfacial effects, they can be tuned independently.

For the discussion of this result, we have to consider that the Co layer is sandwiched between Au and NiO(CoO) and therefore experiences additive interfacial DMI [16] related to the two interfaces Au/Co and Co/NiO(CoO). In view of a theoretical calculation predicting a rather weak negative value of DMI for Au/Co [8] and a strong positive one for Co/(nonmagnetic oxides) interfaces [15,46], our value and its sign are quite surprising, particularly, in view of recent experimental findings, confirming a weak negative value of DMI for Au/Co interface [47]. The large negative value of DMI may therefore only originate from the Co/(CoO)NiO interface, where the spins from the AFM additionally contribute to $\vec{D}_{\mathrm{eff}}$. Note that a strong exchange interaction at the interface between very thin CoO and a thick NiO forces the orientation of the magnetic moments in CoO to follow the orientation of the NiO spins, being responsible for the reduction of the Néel temperature. We do not expect that the ultrathin CoO layer remarkably decreases the Néel temperature of NiO since the Néel temperature of thick NiO in the present stoichiometry is equal to 525 K. Indeed, at RT we found shifted hysteresis loops in the PMOKE measurements indicating the presence of EB and proving AFM ordering of CoO/NiO at RT. We suggest that this additional contribution to DMI comes from the interaction between Ni(Co) (from AFM layer) and Co (from FM layer) atoms mediated by the oxygen atoms. This interaction should be negative and large because it has to overcome the positive contribution to DMI arising from Co(FM) and O atoms [15,46]. Such a system with DMI has not been discussed yet, neither theoretically nor experimentally.

To show that the present thin film system can be used as a medium for a bubblecade or racetrack memory using field-induced domain movement, we controlled the position of the magnetic domains by a sequence of external magnetic field pulses in analogy to the method presented by Moon *et al.* (Fig. 2 in Ref. [11]). Using a magnetic field sequence of $H_x = +900$ Oe, $H_z = +300$ Oe and $H_x = -900$ Oe, $H_z = -300$ Oe, a domain can be controllably moved. We were able to move the domain over a distance of tens of microns after five cycles of magnetic field pulses [Figs. 6(a)–6(e)] with a position precision of a few microns. Here, the negative D_{eff} forces clockwise chirality of N-DWs, the movement direction of the nucleated domain is parallel to the direction of H_x, when the first pulse $+H_z$ is applied. When the same field sequence is applied to a layered system with opposite chirality of the magnetization inside the DWs (opposite sign of D_{eff}), the domain will propagate in the opposite direction. Additionally, the direction of motion is opposite to the reversed polarity of the domains [compare Figs. 3(a) with 3(c) and 3(b) with 3(d)]. In summary, our fundamental findings open a way to control the domain movement. With this method, we expect that the use of magnetic fields oriented along x, y, z coordinates allows to move domains either way between desired positions within a surface plane.

IV. CONCLUSIONS

To conclude, we found that domain walls in an exchange biased Au/Co/NiO polycrystalline film possess clockwise chirality of their magnetic moments arrangement in N-DWs independent of the direction of IEBC. We have shown that the relation between asymmetric DW propagation and Co layer thickness can be used to determine the strength of interfacial DMI. Using this method, we correlated the clockwise chirality with a strong negative interfacial Dzyaloshinskii-Moriya interaction ($D_s = -1.11$ pJ/m). We demonstrated that due to this spin configuration in DWs the domain propagation can be controlled with high precision by homogeneous external magnetic fields simultaneously applied out of plane and in plane. This concept can be attractive for many applications based on field-induced domain motion, especially in systems where exchange bias is required.

ACKNOWLEDGMENTS

The authors would like to thank Professor J. Korecki for valuable discussions. This work was supported by the National Science Centre Poland partially under the Maestro (Grant No. UMO-2011/02/A/ST3/00150) and the SONATA-BIS (Grant No. UMO-2015/18/E/ST3/00557) fundings and by the Polish-German joint project (Grant No. PPP-PL 57154298).

[1] I. Dzyaloshinsky, J. Phys. Chem. Solids **4**, 241 (1958).
[2] T. Moriya, Phys. Rev. **120**, 91 (1960).
[3] M. Bode, M. Heide, K. von Bergmann, P. Ferriani, S. Heinze, G. Bihlmayer, A. Kubetzka, O. Pietzsch, S. Blügel, and R. Wiesendanger, Nature (London) **447**, 190 (2007).
[4] S. Heinze, K. von Bergmann, M. Menzel, J. Brede, A. Kubetzka, R. Wiesendanger, G. Bihlmayer, and S. Blügel, Nat. Phys. **7**, 713 (2011).
[5] S. Emori, U. Bauer, S.-M. Ahn, E. Martinez, and G. S. D. Beach, Nat. Mater. **12**, 611 (2013).
[6] J. Sampaio, V. Cros, S. Rohart, A. Thiaville, and A. Fert, Nat. Nanotechnol. **8**, 839 (2013).
[7] A. Fert and P. M. Levy, Phys. Rev. Lett. **44**, 1538 (1980).
[8] H. Yang, A. Thiaville, S. Rohart, A. Fert, and M. Chshiev, Phys. Rev. Lett. **115**, 267210 (2015).
[9] A. Belabbes, G. Bihlmayer, S. Blügel, and A. Manchon, Sci. Rep. **6**, 24634 (2016).
[10] G. Chen, T. Ma, A. T. N'Diaye, H. Kwon, C. Won, Y. Wu, and A. K. Schmid, Nat. Commun. **4**, 2671 (2013).
[11] K.-W. Moon, D.-H. Kim, S.-C. Yoo, S.-G. Je, B. S. Chun, W. Kim, B.-C. Min, C. Hwang, and S.-B. Choe, Sci. Rep. **5**, 9166 (2015).
[12] K.-W. Moon, D.-H. Kim, S.-G. Je, B. S. Chun, W. Kim, Z. Qiu, S.-B. Choe, and C. Hwang, Sci. Rep. **6**, 20360 (2016).
[13] R. Wiesendanger, Nat. Rev. Mater. **1**, 16044 (2016).

[14] G. Chen, A. Mascaraque, A. T. N'Diaye, and A. K. Schmid, Appl. Phys. Lett. **106**, 242404 (2015).
[15] H. Yang, O. Boulle, V. Cros, A. Fert, and M. Chshiev, arXiv:1603.01847v2.
[16] C. Moreau-Luchaire, C. Moutafis, N. Reyren, J. Sampaio, C. A. F. Vaz, N. V. Horne, K. Bouzehouane, K. Garcia, C. Deranlot, P. Warnicke *et al.*, Nat. Nanotechnol. **11**, 444 (2016).
[17] E. Martinez, L. Torres, N. Perez, M. A. Hernandez, V. Raposo, and S. Moretti, Sci. Rep. **5**, 10156 (2015).
[18] M. Schott, A. Bernand-Mantel, L. Ranno, S. Pizzini, J. Vogel, H. Béa, C. Baraduc, S. Auffret, G. Gaudin, and D. Givord, Nano Lett. **17**, 3006 (2017).
[19] S. S. P. Parkin, M. Hayashi, and L. Thomas, Science **320**, 190 (2008).
[20] I. Polenciuc, A. J. Vick, D. A. Allwood, T. J. Hayward, G. Vallejo-Fernandez, K. O'Grady, and A. Hirohata, Appl. Phys. Lett. **105**, 162406 (2014).
[21] Y. Zhang, X. Zhang, J. Hu, J. Nan, Z. Zheng, Z. Zhang, Y. Zhang, N. Vernier, D. Ravelosona, and W. Zhao, Sci. Rep. **6**, 35062 (2016).
[22] P. Tierno, F. Sagues, T. H. Johansen, and T. M. Fischer, Phys. Chem. Chem. Phys. **11**, 9615 (2009).
[23] A. Ehresmann, D. Lengemann, T. Weis, A. Albrecht, J. Langfahl-Klabes, F. Göllner, and D. Engel, Adv. Mater. **23**, 5568 (2011).
[24] D. Holzinger, I. Koch, S. Burgard, and A. Ehresmann, ACS Nano **9**, 7323 (2015).
[25] A. Ehresmann, I. Koch, and D. Holzinger, Sensors **15**, 28854 (2015).
[26] D. Holzinger, D. Lengemann, F. Göllner, D. Engel, and A. Ehresmann, Appl. Phys. Lett. **100**, 153504 (2012).
[27] J. H. Franken, H. J. M. Swagten, and B. Koopmans, Nat. Nanotechnol. **7**, 499 (2012).
[28] M. Matczak, B. Szymański, M. Urbaniak, M. Nowicki, H. Głowiński, P. Kuświk, M. Schmidt, J. Aleksiejew, J. Dubowik, and F. Stobiecki, J. Appl. Phys. **114**, 093911 (2013).
[29] S. A. Chambers, Surf. Sci. Rep. **39**, 105 (2000).
[30] P. Kuświk, B. Szymański, B. Anastaziak, M. Matczak, M. Urbaniak, A. Ehresmann, and F. Stobiecki, J. Appl. Phys. **119**, 215307 (2016).
[31] S. Oswald and W. Brückner, Surf. Interface Anal. **36**, 17 (2004).
[32] J. Scofield, J. Electron Spectrosc. Relat. Phenom. **8**, 129 (1976).
[33] M. C. Biesinger, B. P. Payne, A. P. Grosvenor, L. W. Lau, A. R. Gerson, and R. S. Smart, Appl. Surf. Sci. **257**, 2717 (2011).
[34] A. N. Mansour, Surf. Sci. Spectra **3**, 231 (1994).
[35] A. P. Grosvenor, M. C. Biesinger, R. S. Smart, and N. S. McIntyre, Surf. Sci. **600**, 1771 (2006).
[36] H. A. Hagelin-Weaver, J. F. Weaver, G. B. Hoflund, and G. N. Salaita, J. Electron Spectrosc. Relat. Phenom. **134**, 139 (2004).
[37] H. A. Hagelin-Weaver, J. F. Weaver, G. B. Hoflund, and G. N. Salaita, J. Alloys Compd. **389**, 34 (2005).
[38] S. Akhter and J. White, Surf. Sci. **180**, 19 (1987).
[39] S.-G. Je, D.-H. Kim, S.-C. Yoo, B.-C. Min, K.-J. Lee, and S.-B. Choe, Phys. Rev. B **88**, 214401 (2013).
[40] A. Hrabec, N. A. Porter, A. Wells, M. J. Benitez, G. Burnell, S. McVitie, D. McGrouther, T. A. Moore, and C. H. Marrows, Phys. Rev. B **90**, 020402 (2014).
[41] E. Jué, C. K. Safeer, M. Drouard, A. Lopez, P. Balint, L. Buda-Prejbeanu, O. Boulle, S. Auffret, A. Schuhl, A. Manchon *et al.*, Nat. Mater. **15**, 272 (2015).
[42] P. Kuświk, M. Matczak, M. Kowacz, F. Lisiecki, and F. Stobiecki, arXiv:1703.05394.
[43] D.-S. Han, N.-H. Kim, J.-S. Kim, Y. Yin, J.-W. Koo, J. Cho, S. Lee, M. Kläui, H. J. M. Swagten, B. Koopmans *et al.*, Nano Lett. **16**, 4438 (2016).
[44] S. Tarasenko, A. Stankiewicz, V. Tarasenko, and J. Ferréb, J. Magn. Magn. Mater. **189**, 19 (1998).
[45] R. Yanes, J. Jackson, L. Udvardi, L. Szunyogh, and U. Nowak, Phys. Rev. Lett. **111**, 217202 (2013).
[46] O. Boulle, J. Vogel, H. Yang, S. Pizzini, D. de Souza Chaves, A. Locatelli, T. O. Menteş, A. Sala, L. D. Buda-Prejbeanu, O. Klein *et al.*, Nat. Nanotechnol. **11**, 449 (2016).
[47] R. Rowan-Robinson, A. Stashkevich, Y. Roussigne, M. Belmeguenai, S.-M. Cherif, A. Thiaville, T. Hase, A. Hindmarch, and D. Atkinson, arXiv:1704.01338v1.